






## *In Silico* Approach: Effect of the Oxidation Iron State (Heme-Group) in Steroidogenesis Pathways

David Mora-Martinez <sup>1</sup> Jorge Organista-Nava <sup>2</sup> Jesús Sandoval-Ramirez <sup>1</sup> Berenice Illades-Aguiar <sup>2</sup> Alan Carrasco-Carballo <sup>1,2\*</sup> 

<sup>1</sup> Laboratorio de Elucidación y Síntesis en Química Orgánica, Facultad de Ciencias Químicas, Benemérita Universidad Autónoma de Puebla, Puebla, Puebla, Mexico

<sup>2</sup> Laboratorio de Biomedicina Molecular, Facultad de Ciencias Químico Biológicas, Universidad Autónoma de Guerrero, Chilpancingo, Guerrero, México

\*email: [alan.carrascoc@correo.buap.mx](mailto:alan.carrascoc@correo.buap.mx)

### Keywords:

CYPs  
Enzyme inhibitors  
Fe state oxidation  
Molecular docking  
Specific inhibitors

### Abstract

One of the main design features of enzyme regulators for the CYPs is the presence of a heme-group and different oxidation states in iron atoms. The selective inhibition of a CYP-enzyme can help to reduce the formation of steroidal molecules that causes undesirable disorders and is, therefore a topic of great biochemical-pharmaceutical interest. The present work carried out an analysis of effect on the coupling-energy of the iron core according to its changes from oxidation Fe(II) to Fe(III) state, over inhibitors and substrates, in a particular enzyme. Two crystals from CYP21A2, CYP11A1, CYP17A1 and CYP19A1 enzymes were selected, assigning the oxidation states separately in each case. It was highlighted that for CYP11A1 and CYP19A1 enzymes, no significant difference was observed in coupling energies between Fe oxidation state and crystal stereo-disposition. This last can be used to analyze their congruence towards the reported biological data. For CYP17A1, the ideal crystal for inhibitors design is 6CHI since the crystal with 4NKV presented differences in all the molecules analyzed since the oxidation state of the iron atom changes the molecule's orientation in the enzyme coupling. In contrast, in CYP21A2, no changes were observed. A greater biological congruence with 5BVU was observed because the coupling energies concur with the selectivity of the enzyme towards its endogenous substrates and reported inhibitors. It was concluded that the effect of the oxidation state of iron on the Binding Coupling Energy (BCE) depends directly on the functional groups attached to the steroidal molecule and their stereo-disposition.

Received: May 19<sup>th</sup>, 2022

Revised: June 27<sup>th</sup>, 2022

Accepted: June 29<sup>th</sup>, 2022

Published: June 30<sup>th</sup>, 2022



© 2022 David Mora-Martinez, Jorge Organista-Nava, Jesús Sandoval-Ramirez, Berenice Illades-Aguiar, Alan Carrasco-Carballo. Published by Institute for Research and Community Services Universitas Muhammadiyah Palangkaraya. This is an Open Access article under the CC-BY-SA License (<http://creativecommons.org/licenses/by-sa/4.0/>). DOI: <https://doi.org/10.33084/jmd.v2i1.3548>

## INTRODUCTION

Iron is present in the human body, having many biological functions; for example, as a coordination metal with molecular oxygen, on the heme group of hemoglobin, being a decisive couple for cell oxygenation<sup>1-3</sup>. The cytochrome P450 (CYP) enzymes are membrane-bound hemoproteins involved in oxidative processes leading to the activation or inactivation of many endogenous and exogenous chemicals in mammals and plants. These enzymes play a critical role in xenobiotic detoxification, cellular metabolism, and homeostasis<sup>3</sup>. CYPs play essential roles in dehydrogenation and oxidative processes; in these last, for example, by adding hydroxyl groups in specific positions of molecules. CYP17A1 hydroxylates the 17 $\alpha$  pregnane position stereoselectively or oxidizes the pregnane side chain at C-17 to produce the 17-oxo function, in which two carbon atoms are eliminated. A similar process occurs with CYP11A1, CYP19A1, and CYP21A2 (Figure 1)<sup>4,5</sup>. This catalytic process is assisted by NADH and NAD, in which the initial Fe(III) changes towards different oxidation states. In this cycle, the substrate (RH or ROH) is coupled to Fe(III) and reduced

to Fe(II), maintaining the complex with the substrate; then, an oxygen molecule binds to the Fe(II) complex until the oxidation process is completed to form the product (RH(R)ROH or ROH(R)R=O) (Figure 2). The critical step occurs in the reduction step Fe(III) to Fe(II) since the complex must be sufficiently stable to accomplish the catalytic process<sup>2,6,7</sup>.

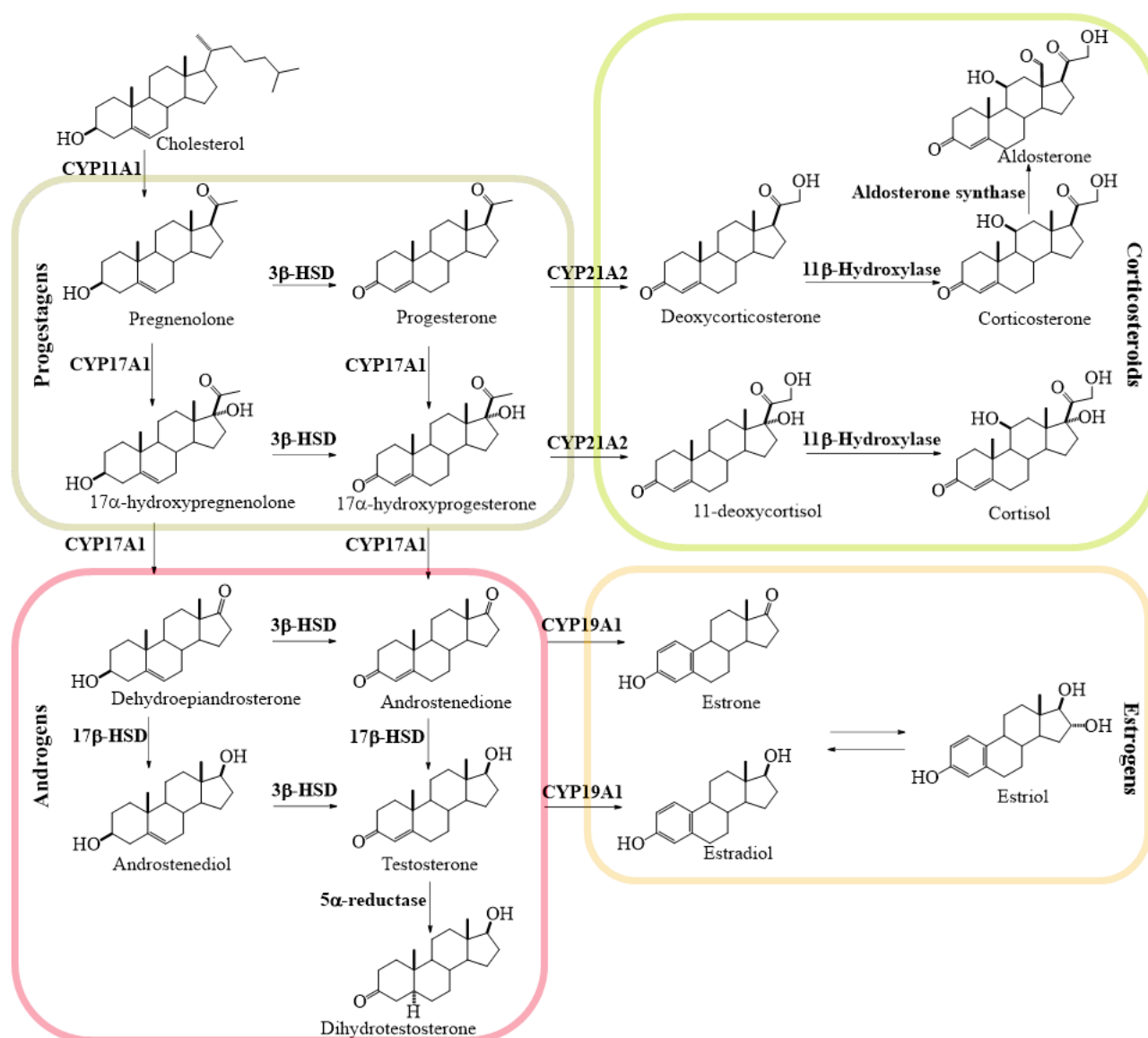
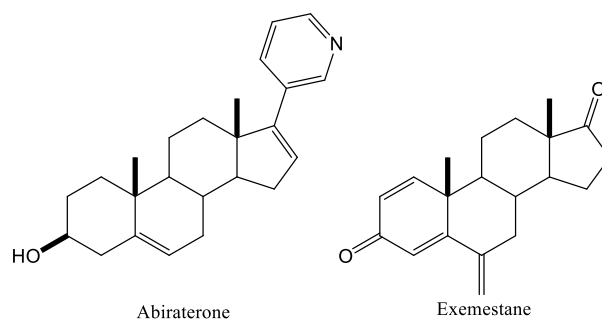


Figure 1. Cholesterol steroidogenesis<sup>4,8</sup>.

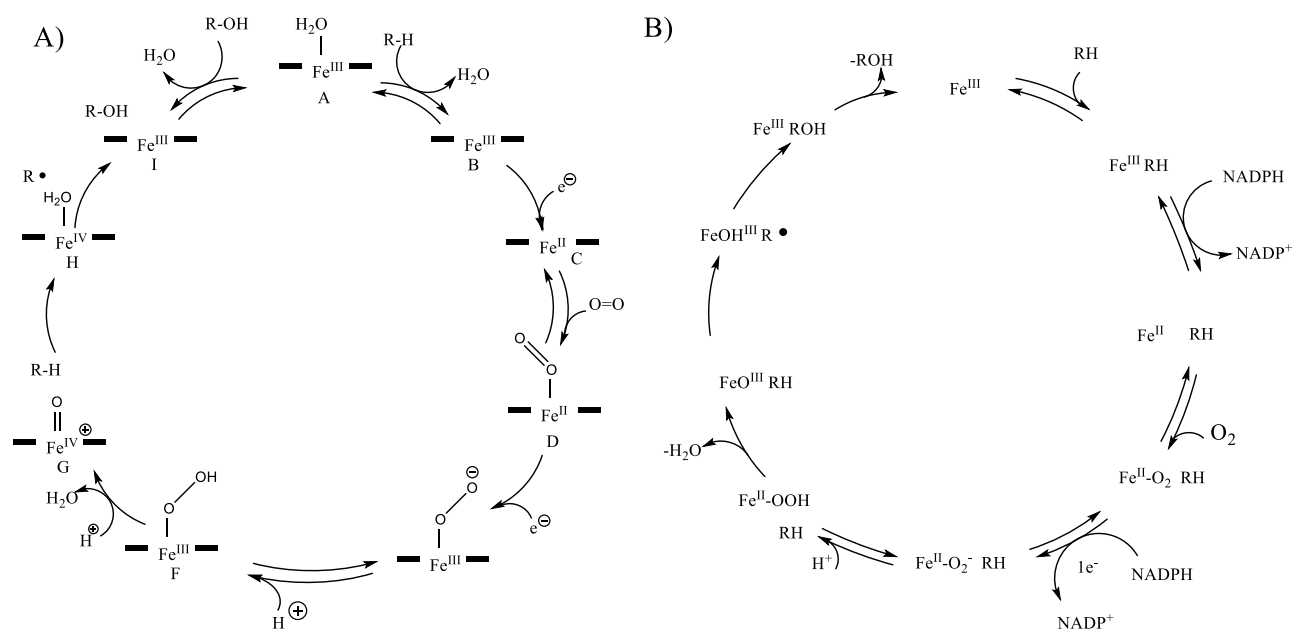
Cholesterol steroidogenesis is related to the development of hormone-dependent cancers (prostate, testicle, breast, cervix), for which inhibitors are continuously sought<sup>9,10</sup>. This has led to searching for drugs against the related enzymes shown in the steroidogenesis map (Figure 1). The commercial drug abiraterone was designed to inhibit CYP17A1, but it produces undesirable side effects; it lacks selectivity, simultaneously inhibiting CYP21A2<sup>10,11</sup>. For CYP19A1, exemestane is available, but it has a low affinity to CYPs, and therefore this drug exhibits low inhibition constant ( $K_i$ ); so, its inhibitory effect is attenuated at high concentrations of the substrate<sup>12,13</sup>. Also, specific mutations or non-selective inhibitions of steroidogenic CYPs are related to various pathologies<sup>8,9,14</sup>.

CYP11A1's deletion completely stops steroid hormone production, generating hermaphroditism, osteoporosis, cryptorchidism, and sterility. CYP17A1 inhibition generates congenital adrenal hyperplasia and hypertension. CYP19A1 inhibition induces osteoporosis and virilization in women due to increased production of androgens<sup>5,15</sup>. Mutations or inhibition of CYP21A2 generates congenital adrenal hyperplasia, perineal hypospadias, chordee, hyperandrogenism, and decreases corticosteroid production<sup>16,17</sup>.



**Figure 2.** CYPs inhibitors references.

The importance of the biological mechanism of the steroidogenic CYPs lies in its chemo-, diastereo- and stereoselective steroid oxidation. Although the general catalytic cycle of CYPs<sup>11,18</sup> indicates only the transformation Fe(III) to Fe(II)<sup>4,18</sup>, the cycle for CYP19A1 includes the presence of Fe(IV); but both converge in the critical step (**Figure 3**), which is found in the change from Fe(III) to Fe(II)<sup>19</sup>. Until now, the design of *in silico* inhibitors for CYP11A1<sup>20</sup>, CYP17A1<sup>21</sup>, CYP19A1<sup>22</sup>, and CYP21A2<sup>23</sup> has only been focused on the basal form of the enzyme<sup>24,25</sup>. However, the effect of changes in their binding coupling energy (BCE) is crucial to explain the selectivity of inhibitors in a catalytic process compared to their natural substrates; this last is the objective of this work.



## MATERIALS AND METHODS

### Hardware and Software

The hardware used was PC Inter® Core™ i9-10900 RAM 64.00 GB @2.80 GHz, Windows 10-64 bit, Chem3D 17.1, Discovery Studio® (<https://www.3ds.com/>), AutoDockTools® (<https://ccsb.scripps.edu/mgltools/>)<sup>26</sup> and AutoDock Vina (<http://vina.scripps.edu/>)<sup>27</sup>.

### Co-Crystals/Ligands

Substrates and inhibitors were obtained from the Protein Data Bank (<https://www.rcsb.org/>) as co-crystals with the CYPs, cholesterol (PDB ID 3N9Y), (22R)-OH-cholesterol (3N9Z), dihydroxycholesterol (3NA0), (20S)-OH-cholesterol (3NA1)<sup>28</sup>, abiraterone (4NKV), 17 $\alpha$ -OH-pregnenolone (4NKz), 17 $\alpha$ -OH-progesterone (4NKY), pregnenolone (4NKW), progesterone (4NKX)<sup>29</sup>, 3 $\beta$ -hydroxy-17-(3-pyridyl)androsta-5,16-diene 6-carboxamide (6CHI), 3 $\beta$ -hydroxy-

17-(3-pyridyl)-5 $\alpha$ -androst-16-en-6-one oxime (6CIR), 3 $\beta$ -hydroxy-17-(3-pyridyl)androsta-5,16-diene 6-carbonitrile (6CIZ)<sup>11</sup>, androstenedione (3EQM)<sup>30</sup>, exemestane (3S7S)<sup>31</sup>, and testosterone (3KDM)<sup>32</sup>. All molecules were energetically and geometrically optimized in Chem3D 17.1 using MM2<sup>33</sup> and PM7<sup>34</sup> (<http://openmopac.net/>).

### CYPs

The CYPs crystals were obtained from the Protein Data Bank (<https://www.rcsb.org/>) with the following identification data (PDB ID): CYP11A1 (3N9Y, 3NA1<sup>28</sup>); CYP17A1 (4NKV, 4NKZ, 4NKX<sup>29</sup>, 6CHI<sup>11</sup>); CYP19A1 (3EQM<sup>30</sup>, 5JKV<sup>35</sup>, 3S7S<sup>36</sup>, 4GL5<sup>31</sup>); and CYP21A2 (4Y8W, 5VBU<sup>37</sup>). They were prepared and optimized by assigning polar hydrogens to a histidine protonation state, the iron atom charge was assigned using AutoDockTools<sup>26</sup>.

### Docking Protocol

Molecular docking was performed in AutoDock Vina<sup>27</sup>, validating firstly each one of the proteins and their co-crystallized substrate/inhibitor, taking a root mean square deviation (RMSD) <1.0 Å as the cut-off limit, and then incorporating iron under diverse oxidation states for all possible inhibitors and substrates.

### Assessment

The selection of enzyme crystals was carried out according to the quality of each crystal and co-crystallized inhibitor or substrate. Later, proteins were prepared to assign charges II or III for the iron atom of each enzyme and compare their best binding couple energy (BCE), according to the oxidation state and the associated protein, as well as the selectivity vs. other proteins, to finally analyze the chemical environment around the heme group in each case.

## RESULTS AND DISCUSSION

Data availability for CYP11A1, CYP17A1, CYP19A1, and CYP21A2 crystals is extensively described in different databases, permitting the selection of suitable crystals for the inhibitor design. Additionally, it is crucial to know how it inhibits the enzyme, being of particular interest the oxidation state change in the first step of the mechanism. Even if all proteins share the same redox process, the nature of the pocket in each enzyme is different, presenting a particular effect with the endogenous substrate or co-crystallized inhibitors<sup>38</sup>.

For CYP11A1, two crystals were prepared for each oxidation state; it is denoted that there was no change in the coupling energy. A slight decrease in energy (although not significant) is observed between the crystals. Both were co-crystallized with endogenous substrates presenting an ideal conformation for competitive inhibition. The CYP11A1 enzymatic activity presented a lower coupling energy than the substrates, which explains how it is displaced and released by the new substrate molecule after being converted. For the 3N9Z crystal, there are minimal changes of the order of 0.1 kcal/mol for the substrates, while for the 3NA1 crystal, they remain constant, indicating that the oxidation state in the first reaction step is not significant in the design of the competitive inhibitors for this enzyme. It is also highlighted that abiraterone (CYP17A1 inhibitor) has a higher energy than natural substrates, which places it as a possible inhibitor of this enzyme, highlighting possible side effects (**Table I**). In the case of the cholestane side chain oxidation in the steroidogenesis, the steroid molecules interact with the heme group in two steps: firstly, the insertion of a hydroxyl group, and secondly, in a further interaction its fragmentation is realized, giving rise to a pregnane side chain. **Figure 4** shows minimal changes in the steroid's position according to the iron atom's different oxidation states, which explains the similar values in their BCE.

**Table I.** Effect on the coupling energy in the CYP11A1 according to the oxidation state of iron in the heme group.

Molecule/PDB-ID	3N9Z		3NA1	
	III	II	III	II
Cholesterol	-11.1	-11.2	-11.5	-11.5
(20S)-hydroxycholesterol	-11.4	-11.3	-11.7	-11.7
Dihydroxycholesterol	-11.5	-11.5	-11.6	-11.6
(22R)-hydroxycholesterol	-11.4	-11.5	-11.8	-11.8
Abiraterone	-11.9	-11.9	-12.0	-12.0
Progesterone	-10.8	-10.8	-10.7	-10.7
Pregnenolone	-10.7	-10.7	-10.7	-10.7

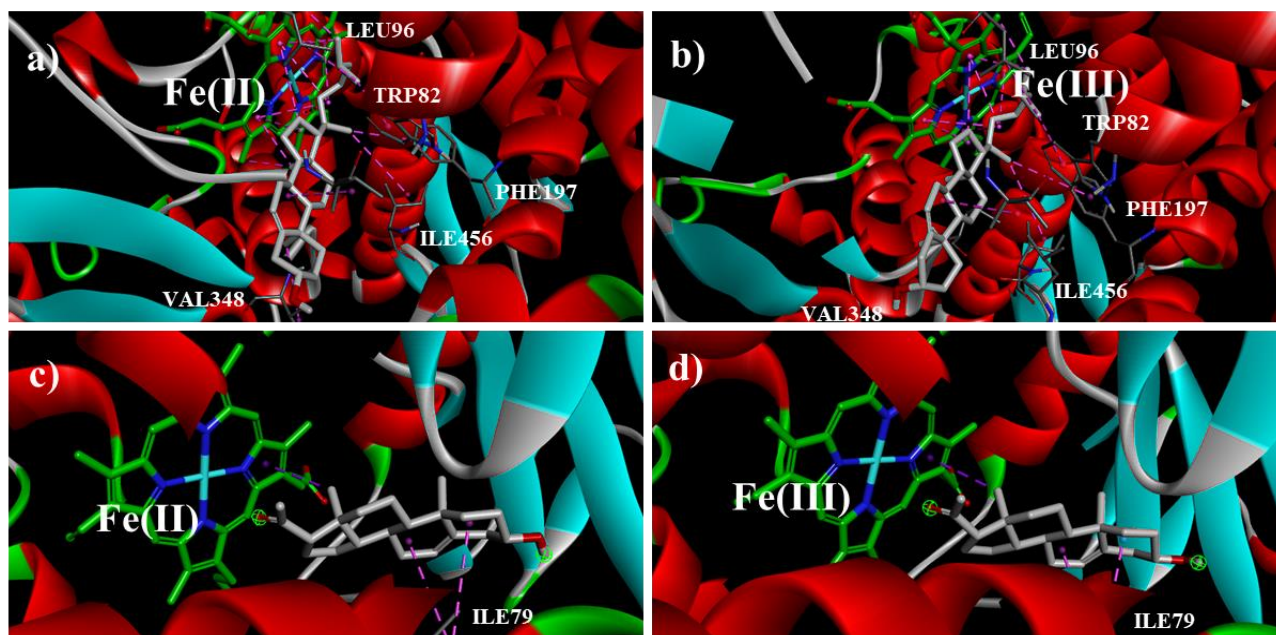


**Figure 4.** Interactions of the CYP11A1 with a) cholesterol, 3N9Z, Fe(II), b) Cholesterol, 3N9Z, Fe(III), c) Pregnenolone, 3N9Z, Fe(II), and d) Pregnenolone, 3N9Z, Fe(III).

In the case of abiraterone, it did not show significant changes in the BCE using the two oxidation states. Both crystals displayed interactions of the rings A and B with Ile84 (blue). However, the interaction between the A ring and Val348 was only present in the 3N9Z crystal and Leu456 (red) in the 3NA1 (**Figure 5**). For rings D and E, only the 3NA1 crystal presented an interaction with the heme group, which corresponds to the literature<sup>11,20</sup> and reflects the importance of the pyridyl ring in its inhibitory activity, as well as its orientation towards the heme group; this difference of the two crystals reflects the three-dimensional conformation of the active site and not the oxidation state<sup>39</sup>.

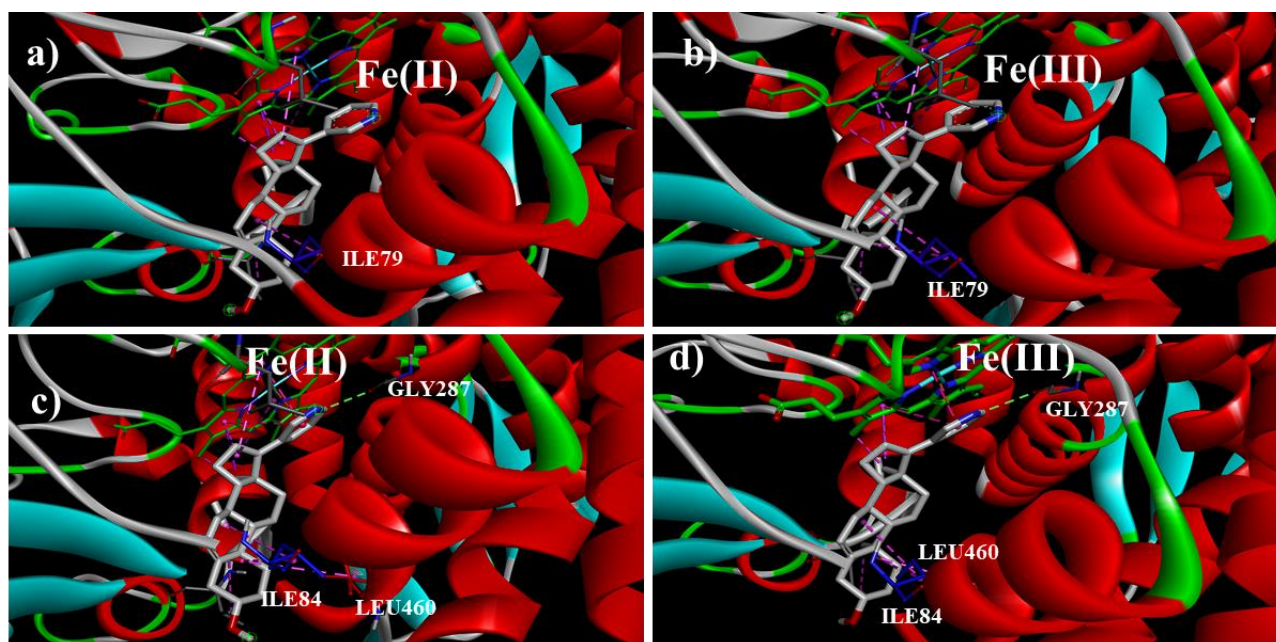


**Figure 5.** Interactions of the abiraterone and the CYP11A1 with a) 3N9Z, Fe(II), b) 3N9Z, Fe(III), c) 3NA1, Fe(II), and d) 3NA1, Fe(III).

On the other hand, the two co-crystals of the CYP17A1 are designed inhibitors pharmacologically proved (**Table II**). In the case of the 6CHI crystal, there are minimal differences according to the charge, with a decreasing tendency in the Fe(II) state. Although independent of the oxidation state, the correlation between energy and the reported inhibitory effect can be demonstrated, noting that the abiraterone (reference drug) has higher energy than the four

natural substrates; the same effect is observed for the other experimental inhibitors. In contrast, for the 4NKV crystal, the oxidation state change generates a significant change in the coupling energy, which decreases by around 50%, maintaining higher coupling energy for the inhibitors than the endogenous substrates; the energy decrease can be explained. Because making the change in the oxidative state, allows a separation for the insertion of oxygen, which will carry out the substrate oxidation, although, in the inhibitors, this change is not favored because it would decrease inhibitory activity<sup>40</sup>.

**Table II.** Effect on the coupling energy at CYP17A1, according to the oxidation state of iron in the heme group.

Molecule/PDB-ID	6CHI		4NKV		
	Fe Charge	III	II	III	
Exemestane		-10.9	-10.8	-11.0	-5.8
Testosterone		-10.5	-10.4	-11.0	-5.3
Progesterone		-11.2	-11.2	-11.7	-5.0
Pregnenolone		-11.0	-11.0	-11.5	-5.2
17 $\alpha$ -OH-progesterone		-11.4	-11.4	-12.0	-5.7
17 $\alpha$ -OH-pregnenolone		-11.1	-11.0	-11.4	-5.5
Abiraterone		-12.2	-12.2	-13.3	-5.6
Amide-abiraterone		-12.8	-12.8	-13.4	-5.5
Nitrile-abiraterone		-12.7	-12.7	-13.3	-5.6
Oxime-abiraterone		-13.3	-13.2	-12.3	-5.8
Androstenedione		-10.6	-10.6	-11.4	-5.7

To explain the energy results, a 3D analysis of the interactions and position of the molecules with the protein crystals was carried out (Figure 6). In the case of coupled with the 6CHI crystal, the interactions responsible for the coupling energy are mainly hydrophobic, between the protein and the steroidal nucleus, and not with the heme group. Therefore, it is explained that iron's oxidation state does not directly impact the BCE. In contrast, in the 4NKV crystal, when changing the oxidation state to Fe(III), it is the A ring that binds to the iron site of the heme group, decreasing the coupling energy considerably<sup>41</sup>. This crystal was crystallized with a reference inhibitor; its conformation is slightly altered, and although it has been widely used for design studies of inhibitors of this enzyme when comparing the results with the endogenous substrates, it would be indicated to use the 6CHI CYP17A1 crystal.

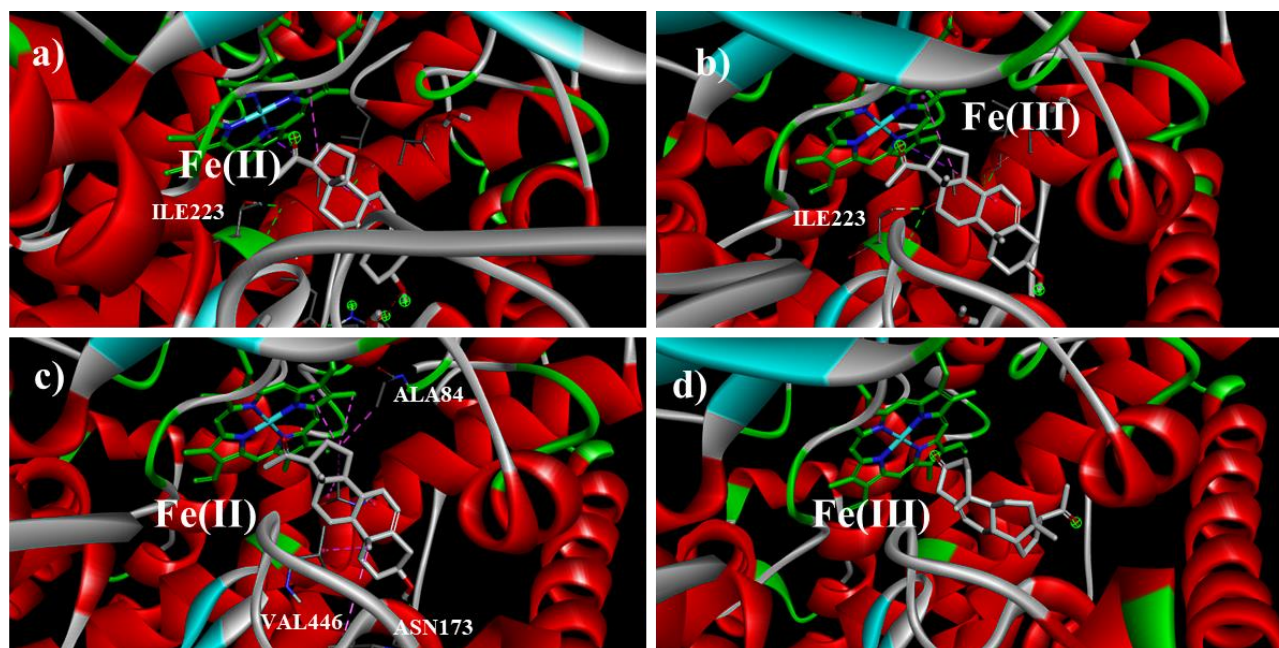


**Figure 6.** Interactions of the pregnenolone and the CYP17A1 with a) 6CHI, Fe(II), b) 6CHI, Fe(III), c) 4NKV, Fe(II), and d) 4NKV, Fe(III).

In contrast to the reference inhibitors for 4NKV (Figure 7), the position of interaction between the pyridine ring and the iron of the heme group is unaltered. The energy decreases in the case of the Fe(III) state because when the oxidation state changes, it loses the pi-cation and pi-pi interaction with the pyrrolic rings of the heme group; the interaction

occurs between Fe(III) with the nitrogen electron pair, due to an increase in the acidity of the iron, increasing the interaction but preventing others, resulting in a lower the coupling energy<sup>42</sup>. In the case of the results obtained in the 6CHI, energetic stability is maintained between the coupling energy independent of the oxidation state, reaffirming the appropriate choice for the design of competitive inhibitors of CYP17A1.

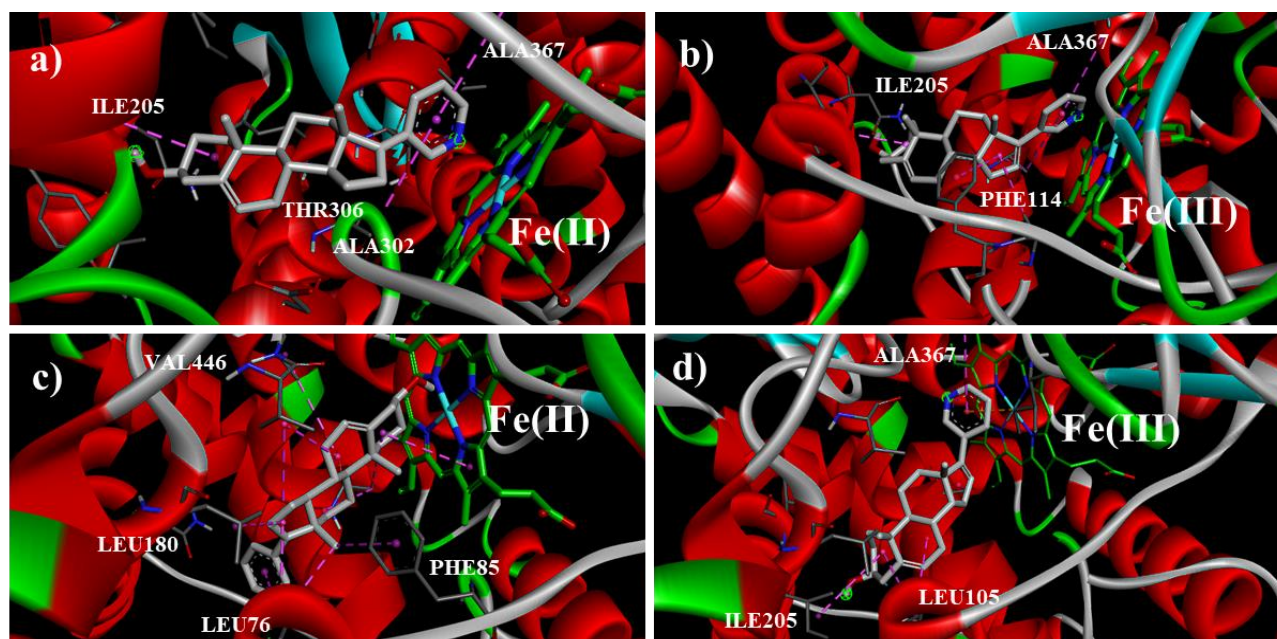


**Figure 7.** Interactions between the abiraterone and the CYP17A1 with a) 6CHI, Fe(II), b) 6CHI, Fe(III), c) 4NKV, Fe(II), and d) 4NKV, Fe(III).

Similarly, for CYP19A1, the molecular docking results show a similar energy level independent of the oxidation state and the crystal used, which makes their use ideal for inhibitor design. Exemestane (reference drug) presents higher coupling energy than the substrates (testosterone and androstenedione), which is consistent with the design of inhibitors. In contrast, abiraterone and its derivatives have lower energy, so they are not inhibitors of this enzyme, but continue to maintain the same energy level between both crystals and oxidation states, except nitrile-abiraterone, which when passing to Fe(II), the energy decreases by 0.3 kcal/mol. In comparison, abiraterone increases by 0.2 kcal/mol; although they are not significant, they must be considered for the design of inhibitors that work independently of the oxidation state in the initial phases of the catalytic cycle (Table III). The high similarity of the coupling energy is due to the interactions between the A and D rings with the heme group's porphyrin and the surrounding sidechains, for both exemestane and androstenedione. Figures 8 and 9 show that regardless of the crystal, the oxygens at C-3 and C-17 form polar interactions with the amino acid sidechains surrounding the heme group and not with it, explaining the absence of a change in the coupling energy.

**Table III.** Effect on the coupling energy in the CYP19A1 according to the oxidation state of iron in the heme group.

Molecule/PDB-ID	3EQM		5JKV	
	III	II	III	II
Exemestane	-14.2	-14.2	-14.2	-14.2
Testosterone	-13.0	-13.0	-13.0	-13.0
Abiraterone	-8.0	-8.2	-8.3	-8.3
Amide-abiraterone	-8.4	-8.4	-7.8	-7.8
Nitrile-abiraterone	-8.1	-8.1	-8.0	-8.0
Oxime-abiraterone	-9.0	-9.0	-8.8	-8.8
Androstenedione	-14.0	-14.0	-14.0	-14.0

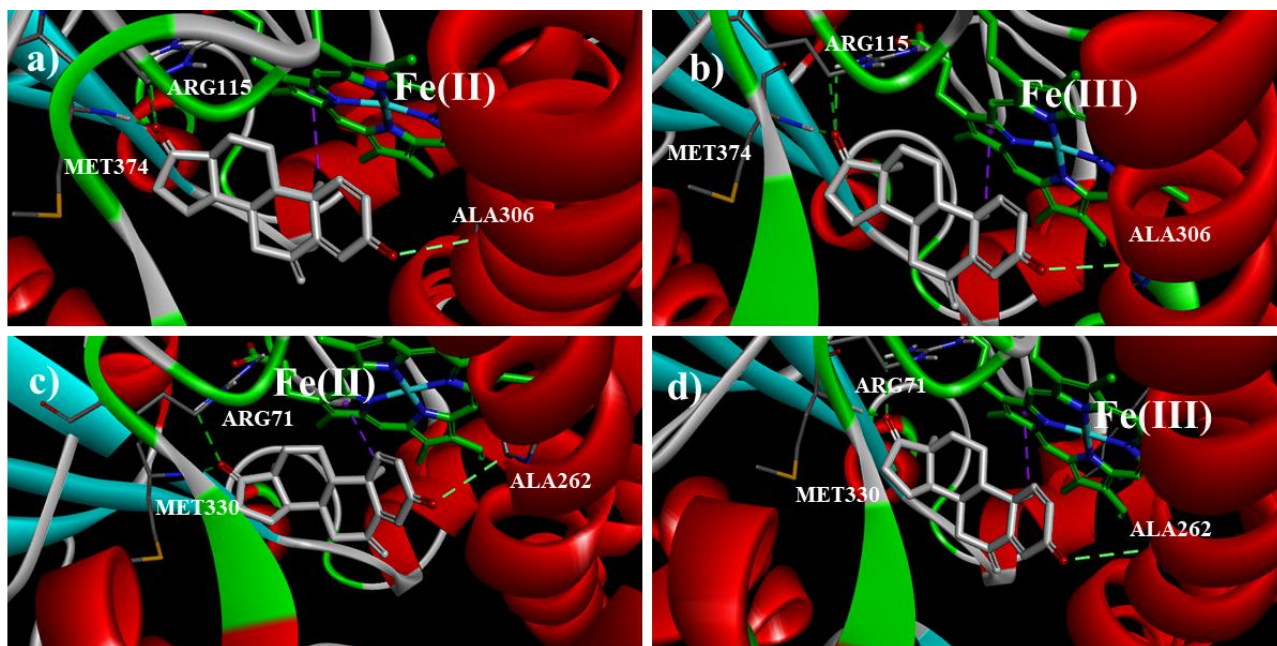


**Figure 8.** Interactions between the exemestane and the CYP19A1 with a) 3EQM, Fe(II), b) 3EQM, Fe(III), c) 5JKV, Fe(II), and d) 5JKV, Fe(III).

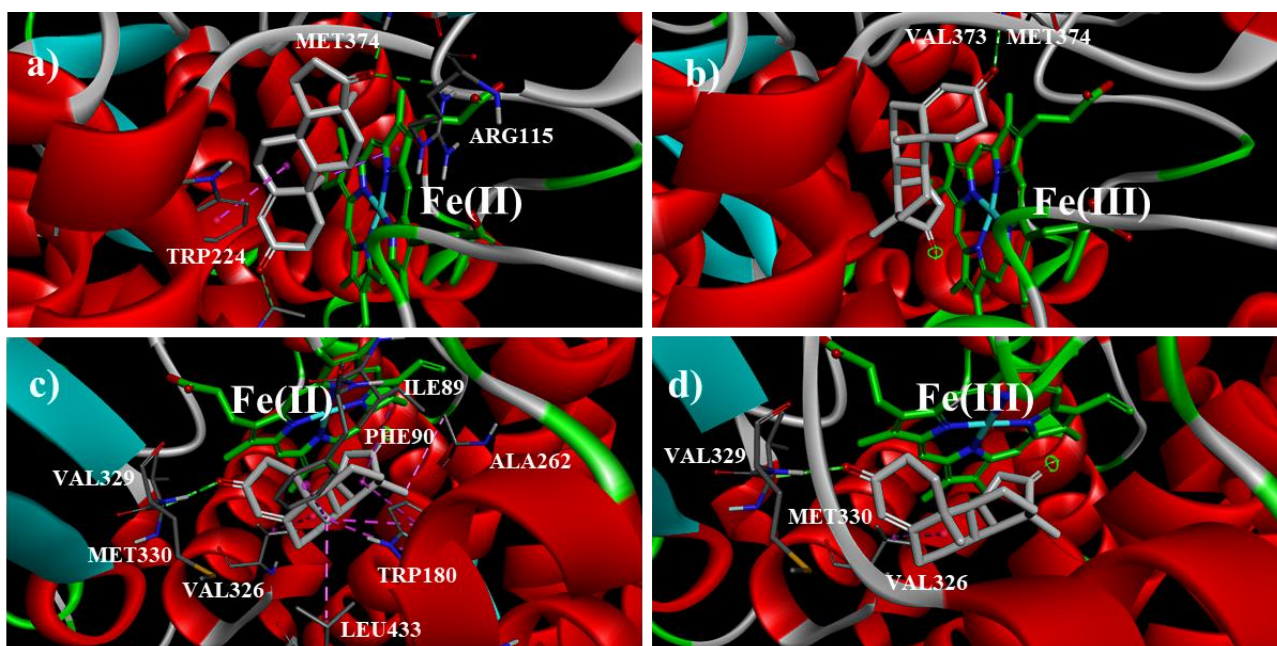


**Figure 9.** Interactions between the androstenedione and the CYP19A1 with a) 3EQM, Fe(II), b) 3EQM, Fe(III), c) 5JKV, Fe(II), and d) 5JKV, Fe(III).

Despite when studying whether CYP17A1 inhibitors could present an adverse effect of competitive inhibition for CYP19A1, they do not reach the same energy level as the substrates and exemestane because their greater interaction does not place them in the specific site, not allowing them to have direct interaction with the heme group. It can be seen in **Figure 10** how the 5JKV crystal interacts with the outer loops, while with the 3EQM crystal, it is the double bond that interacts in the vicinity of the heme group but without a significant effect.



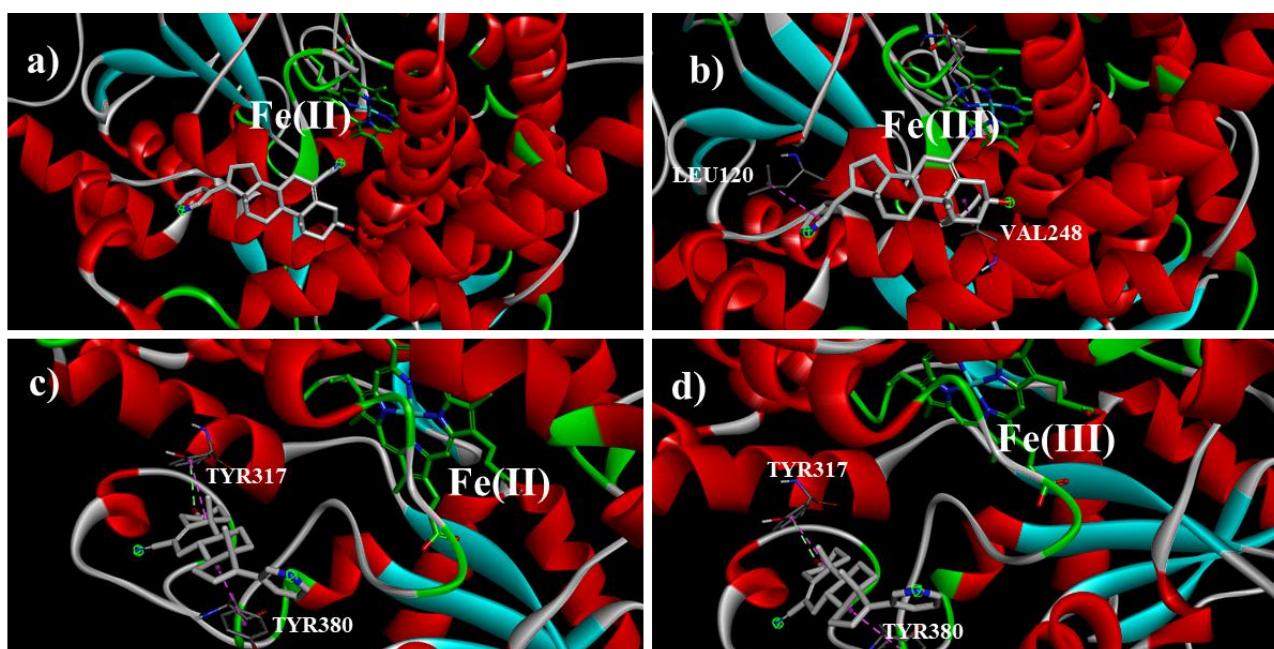


**Figure 10.** Interactions between the derivative nitrile-abiraterone and the CYP19A1 with a) 3EQM, Fe(II), b) 3EQM, Fe(III), c) 5JKV, Fe(II), and d) 5JKV, Fe(III).

In contrast to the previous enzymes, for CYP21A2, the changes generated by the oxidation state and the crystal are considerable. In addition to this, it presents adverse effects with steroidogenesis inhibitors<sup>10,11</sup>. For the natural substrates for the 4Y8W crystal (**Table IV**), the oxidation state is not relevant for the coupling energy, however for the abiraterone, the energy increases when the iron is reduced, which, although it is not higher than the natural substrates, at high doses can generate a competitive effect, similar to the one observed with oxime-abiraterone. On the other hand, for the 5BVU crystal, in all cases, a change in coupling energy is observed, decreasing for natural substrates and increasing in inhibitors, particularly for abiraterone producing an increase of 0.4 and 1.0 kcal/mol for the oxime-abiraterone derivative. For the above, for competitive inhibition purposes, the 5BVU crystal is adequate, while for complete inhibition, 4Y8W is a better fit because the oxidation state has less effect on the coupling energy. However, it was to be considered how the impact of the oxidation state of iron is fundamental for the inhibitors design of CYP21A2 or specific inhibition of the rest of steroidogenesis.

**Table IV.** Effect on the coupling energy in the CYP21A1 according to the oxidation state of iron in the heme group.

Molecule/PDB-ID Fe Charge	4Y8W		5BVU	
	III	II	III	II
17 $\alpha$ -OH-progesterone	-12.0	-12.0	-12.8	-12.0
Progesterone	-12.2	-12.2	-11.8	-11.8
Abiraterone	-10.4	-10.8	-10.5	-10.9
Amide-abiraterone	-10.2	-10.2	-8.8	-8.8
Nitrile-abiraterone	-10.2	-10.2	-8.9	-8.9
Oxime-abiraterone	-10.3	-10.9	-10.0	-11.0

The observed interactions in the change of coupling energy (**Figure 11**) are clearly due to the direct interaction between the oxygen of the ketone in C-21 with the iron atom, which generates small changes when increasing to Fe (III). It was also observed that a greater distance in 4Y8W than in 5BVU due to the co-crystals being the initial and final phases of the hydroxylation mechanism. In the case of abiraterone, which has shown adverse effects on the CYP21A2, the pyrimidine ring is orientated to the heme group, except in the case of the 5BVU crystal and Fe(III), where the interaction occurs with the A ring, which generates a change in the coupling energy, in addition to this, it is observed that the B and C rings form interactions with the Trp 202 residue (**Figure 12**).

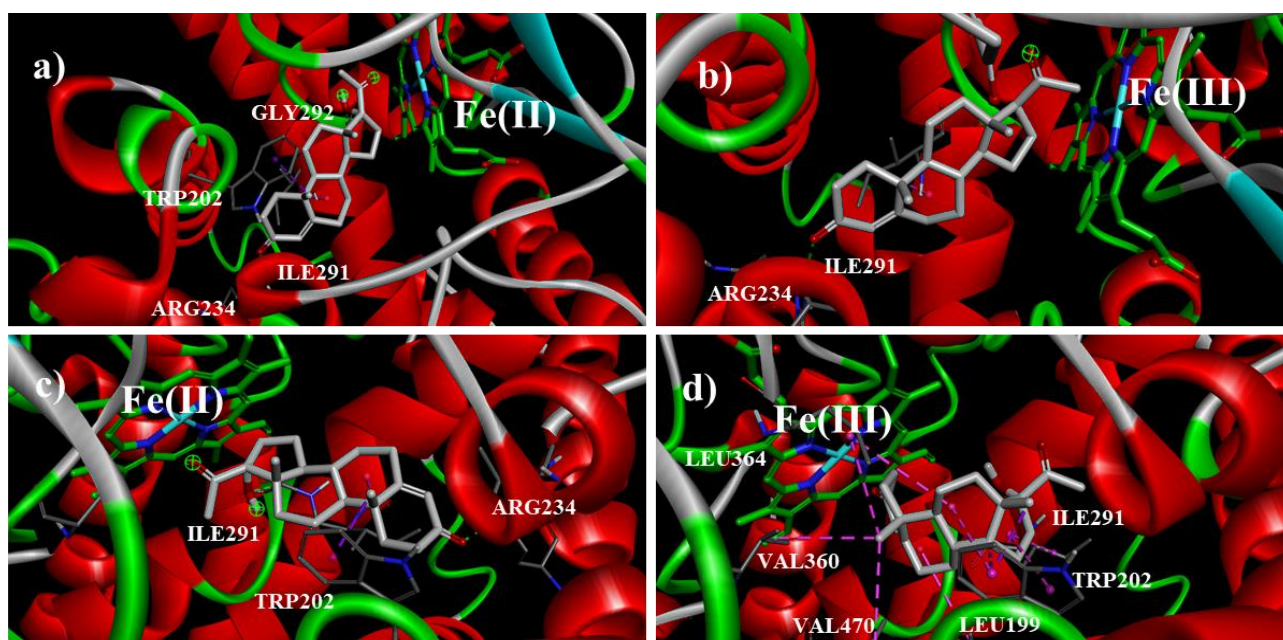


Figure 11. Interactions between the 17 $\alpha$ -OH-progesterone and the CYP21A1 with a) 4Y8W, Fe(II), b) 4Y8W, Fe(III), c) 5VBU, Fe(II), d) 5VBU, Fe(III).

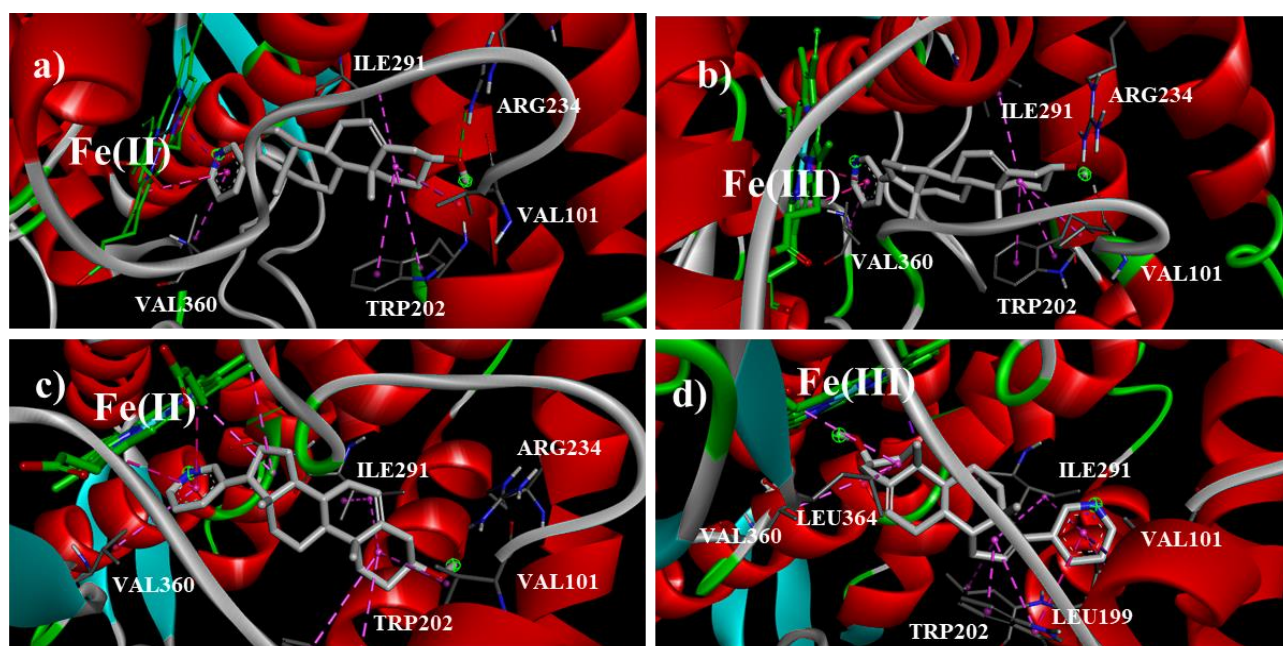


Figure 12. Interactions between the abiraterone and the CYP21A1 with a) 4Y8W, Fe(II), b) 4Y8W, Fe(III), c) 5VBU, Fe(II), and d) 5VBU, Fe(III).

## CONCLUSION

The effect of the oxidation state of the iron atom on the BCE depends on the functional groups present in the analyzed molecule and its orientation with respect to the heme group. Groups having direct interaction with the iron atom have a more significant effect. Of the eight investigated crystals, CYP11A1 presented no energy differences with the Fe(III) and Fe(II) oxidation states. CYP17A1 had a marked difference on the 4NKV crystal, which was absent on the 6CHI. Therefore, *in silico* inhibitor design for this enzyme is suggested using 6CHI. For the CYP19A1, only the abiraterone presented an energy difference, having a better coupling energy for the Fe(II), which was a result of the direct interaction with the pyridyl ring; because of this little difference, both crystals can be used for inhibitor design. In the case of CYP21A2, 17 $\alpha$ -OH-progesterone had a higher BCE (0.8 kcal/mol) with Fe(III) in the 5VBU crystal; abiraterone

also had a higher coupling energy (0.4 kcal/mol in both crystals) but with the Fe(II) state; and the oxime-abiraterone derivative had a greater BCE (0.6 kcal/mol for 4Y8W and of 1.0 kcal/mol for 5VBU) on Fe(II). Therefore, both crystals can be used to design a selective inhibitor, understanding that by choosing the oxidation state of the iron, we are also selecting the phase of the catalytic cycle in which the inhibition will occur. The oxidation state will define in which phase of the catalytic cycle the interaction is being evaluated, so it is essential to carry out a previous study of the enzyme being analyzed. Therefore, for an *in silico* inhibitor design, it is necessary to define which phase of the catalysis to inhibit and which oxidation state of the iron will be used. Otherwise, there is a risk of having results corresponding to another cycle phase.

## ACKNOWLEDGMENT

DMM was the recipient of a mastery fellowships from CONACYT (CVU/Becario: 1095504/788789).

## CONFLICT OF INTEREST

The authors have no conflicts of interest to declare that are relevant to the content of this article.

## FUNDING

This work was partially supported by the National Council of Science and Technology of México [CONACYT; Grants FORDECYT-PRONACES/1717349/2020 (JON)].

## DATA AVAILABILITY

All data are available in the main text.

## AUTHORS' CONTRIBUTIONS

Conceptualization: **ACC**; Data curation: **DMM**; Formal analysis: **ACC**; Funding acquisition: **ACC, JON**; Investigation: **DMM, JSR**; Methodology: **ACC**; Software: **ACC**; Supervision: **BIA, JSR**; Validation: **ACC**; Visualization: **DMM**; Writing – original draft: **ACC, DMM**; Writing – review & editing: All authors.

## REFERENCES

1. Bozkurt S, Gumus I, Arslan H. Dinuclear and mononuclear oxorhenium(V) complexes chelated with the S<sub>2</sub>O bidentate thiourea ligand: Synthesis, crystal structure and catalytic activity. *J Organomet Chem.* 2019;884:66-76. doi:10.1016/j.jorganchem.2019.01.015
2. Esteves F, Rueff J, Kranendonk M. The Central Role of Cytochrome P450 in Xenobiotic Metabolism – A Brief Review on a Fascinating Enzyme Family. *J Xenobiot.* 2021;11(3):94–114. doi:10.3390/jox11030007
3. Manikandan P, Nagini S. Cytochrome P450 Structure, Function and Clinical Significance: A Review. *Curr Drug Targets.* 2017;19(1):38–54. doi:10.2174/1389450118666170125144557
4. Liu Y, Grinkova Y, Gregory MC, Denisov IG, Kincaid JR, Sligar SG. Mechanism of the Clinically Relevant E305G Mutation in Human P450 CYP17A1. *Biochemistry.* 2021;60(43):3262–71. doi:10.1021/acs.biochem.1c00282
5. Porubek D. CYP17A1: A Biochemistry, Chemistry, and Clinical Review. *Curr Top Med Chem.* 2013;13(12):1364–84. doi:10.2174/1568026611313120002

6. Yablokov EO, Sushko TA, Kaluzhskiy LA, Kavaleuski AA, Mezentsev YV, Ershov PV, et al. Substrate-induced modulation of protein-protein interactions within human mitochondrial cytochrome P450-dependent system. *J Steroid Biochem Mol Biol.* 2021;208:105793. doi:10.1016/j.jsbmb.2020.105793
7. Kim D, Rahaman SMW, Mercado BQ, Poli R, Holland PL. Roles of Iron Complexes in Catalytic Radical Alkene Cross-Coupling: A Computational and Mechanistic Study. *J Am Chem Soc.* 2019;141(18):7473-85. doi:10.1021/jacs.9b02117
8. Thieffry C, Wynendaele MV, Aynaci A, Maja M, Dupuis C, et al. AG-205 upregulates enzymes involved in cholesterol biosynthesis and steroidogenesis in human endometrial cells independently of PGRMC1 and related MAPR proteins. *Biomolecules.* 2021;11(10):1472-89. doi:10.3390/biom11101472
9. Capper CP, Rae JM, Auchus RJ. The Metabolism, Analysis, and Targeting of Steroid Hormones in Breast and Prostate Cancer. *Horm Cancer.* 2016;7(3):149-64. doi:10.1007/s12672-016-0259-0
10. Blecharz-Klin K, Szejder-Pacholek A, Wawer A, Pyrzanowska J, Piechal A, Joniec-Maciejak I, et al. Early exposure to paracetamol reduces level of testicular testosterone and changes gonadal expression of genes relevant for steroidogenesis in rats offspring. *Drug Chem Toxicol.* 2022;45(4):1862-9. doi:10.1080/01480545.2021.1892941
11. Fehl C, Vogt CD, Yadav R, Li K, Scott EE, Aubé J. Structure-Based Design of Inhibitors with Improved Selectivity for Steroidogenic Cytochrome P450 17A1 over Cytochrome P450 21A2. *J Med Chem.* 2018;61(11):4946-60. doi:10.1021/acs.jmedchem.8b00419
12. Verma G, Khan MF, Akhtar W, Alam MM, Akhter M, Shaquiquzzaman M. Molecular interactions of bisphenols and analogs with glucocorticoid biosynthetic pathway enzymes: an in silico approach. *Toxicol Mech Methods.* 2018;28(1):45-54. doi:10.1080/15376516.2017.1356415
13. Tiwari N, Pandey A, Kumar A, Mishra A. Computational models reveal the potential of polycyclic aromatic hydrocarbons to inhibit aromatase, an important enzyme of the steroid biosynthesis pathway. *Comput Toxicol.* 2021;19:100176. doi:10.1016/j.comtox.2021.100176
14. Claahsen-van der Grinten HL, Speiser PW, Ahmed SF, Arlt W, Auchus RJ, Falhammar H, et al. Congenital Adrenal Hyperplasia-Current Insights in Pathophysiology, Diagnostics, and Management. *Endocr Rev.* 2022;43(1):91-159. doi:10.1210/endrev/bnab016
15. Bernhardt R, Neunzig J. Underestimated reactions and regulation patterns of adrenal cytochromes P450. *Mol Cell Endocrinol.* 2021;530:111237. doi:10.1016/j.mce.2021.111237
16. Concolino P, Costella A. Congenital Adrenal Hyperplasia (CAH) due to 21-Hydroxylase Deficiency: A Comprehensive Focus on 233 Pathogenic Variants of CYP21A2 Gene. *Mol Diagn Ther.* 2018;22(3):261-80. doi:10.1007/s40291-018-0319-y
17. Gangodkar P, Khadilkar V, Raghupathy P, Kumar R, Dayal AA, Dayal D, et al. Clinical application of a novel next generation sequencing assay for CYP21A2 gene in 310 cases of 21- hydroxylase congenital adrenal hyperplasia from India. *Endocrine.* 2021;71(1):189-98. doi:10.1007/s12020-020-02494-z
18. Teschke R, Neuman MG, Liangpunsakul S, Seitz HK. Alcoholic Liver Disease and the co-triggering Role of MEOS with Its CYP 2E1 Catalytic Cycle and ROS. *Arch Gastroenterol Res.* 2021;2(1):9-25. doi:10.33696/Gastroenterology.2.022
19. Magnani L, Frige G, Gadaleta RM, Corleone G, Fabris S, Kempe MH, et al. Acquired CYP19A1 amplification is an early specific mechanism of aromatase inhibitor resistance in ER $\alpha$  metastatic breast cancer. *Nat Genet.* 2017;49(3):444-50. doi:10.1038/ng.3773

20. Masamrekh RA, Filippova TA, Haurychenka YI, Sherbakov KA, Veselovsky AV, Shumyantseva VV, et al. The interactions of a number of steroid-metabolizing cytochromes P450 with abiraterone D4A metabolite: spectral analysis and molecular docking. *Steroids*. 2020;162:108693. doi:10.1016/j.steroids.2020.108693
21. Abdi SAH, Ali A, Sayed SF, Ahsan MJ, Tahir A, Ahmad W, et al. Morusflavone, a new therapeutic candidate for prostate cancer by cyp17a1 inhibition: Exhibited by molecular docking and dynamics simulation. *Plants*. 2021;10(9):1912. doi:10.3390/plants10091912
22. Giampietro L, Gallorini M, Gambacorta N, Ammazalorso A, De Filippis B, Valle AD, et al. Synthesis, structure-activity relationships and molecular docking studies of phenyldiazenyl sulfonamides as aromatase inhibitors. *Eur J Med Chem*. 2021;224:113737. doi:10.1016/j.ejmech.2021.113737
23. Ahmad S, Khan MF, Parvez S, Akhtar M, Raisuddin S. Molecular docking reveals the potential of phthalate esters to inhibit the enzymes of the glucocorticoid biosynthesis pathway. *J Appl Toxicol*. 2017;37(3):265–77. doi:10.1002/jat.3355
24. Palermo G, Spinello A, Saha A, Magistrato A. Frontiers of metal-coordinating drug design. *Expert Opin Drug Discov*. 2021;16(5):497–511. doi:10.1080/17460441.2021.1851188
25. Dawood HM, Ibrahim RS, Shawky E, Hammada HM, Metwally AM. Integrated in silico-in vitro strategy for screening of some traditional Egyptian plants for human aromatase inhibitors. *J Ethnopharmacol*. 2018;224:359–72. doi:10.1016/j.jep.2018.06.009
26. Morris G, Huey R, Lindstrom W, Sanner MF, Belew RK, Goodsell DS, et al. AutoDock4 and AutoDockTools4: Automated Docking with Selective Receptor Flexibility. *J Comput Chem*. 2009;30(16):2785–91. doi:10.1002/jcc.21256
27. Allouche AR. Gabedit – A Graphical User Interface for Computational Chemistry Softwares. *J Comput Chem*. 2010;32(1):174–82. doi:10.1002/jcc.21600
28. Strushkevich N, MacKenzie F, Cherkesova T, Grabovec I, Usanov S, Park HW. Structural basis for pregnenolone biosynthesis by the mitochondrial monooxygenase system. *Proc Natl Acad Sci U S A*. 2011;108(25):10139–43. doi:10.1073/pnas.1019441108
29. Petrunak EM, DeVore NM, Porubsky PR, Scott EE. Structures of human steroidogenic cytochrome P450 17A1 with substrates. *J Biol Chem*. 2014;289(47):32952–64. doi:10.1074/jbc.m114.610998
30. Ghosh D, Griswold J, Erman M, Pangborn W. Structural basis for androgen specificity and oestrogen synthesis in human aromatase. *Nature*. 2009;457(7226):219–23. doi:10.1038/nature07614
31. Ghosh D, Lo J, Morton D, Valette D, Xi J, Griswold J, et al. Novel aromatase inhibitors by structure-guided design. *J Med Chem*. 2012;55(19):8464–76. doi:10.1021/jm300930n
32. Niemi MH, Takkinen K, Amundsen LK, Söderlund H, Rouvinen J, Höyhty M. The testosterone binding mechanism of an antibody derived from a naïve human scFv library. *J Mol Recognit*. 2011;24(2):209–19. doi:10.1002/jmr.1039
33. Fernández B, Ríos MA, Carballeira L. Molecular mechanics (MM2) and conformational analysis of compounds with N-C-O units. Parametrization of the force field and anomeric effect. *J Comput Chem*. 1991;12(1):78–90. doi:10.1002/jcc.540120109
34. Stewart JJP. Optimization of parameters for semiempirical methods VI: More modifications to the NDDO approximations and re-optimization of parameters. *J Mol Model*. 2013;19(1):1–32. doi:10.1007/s00894-012-1667-x
35. Ghosh D, Egbuta C, Lo J. Testosterone complex and non-steroidal ligands of human aromatase. *J Steroid Biochem Mol Biol*. 2010;181:11–9. doi:10.1016/j.jsbmb.2018.02.009

36. Snyder PW, Mecinovic J, Moustakas DT, Thomas 3<sup>rd</sup> SW, Harder M, Mack ET, et al. Mechanism of the hydrophobic effect in the biomolecular recognition of arylsulfonamides by carbonic anhydrase. *Proc Natl Acad Sci U S A*. 2011;108(44):17889–94. doi:[10.1073/pnas.1114107108](https://doi.org/10.1073/pnas.1114107108)
37. Pallan PS, Wang C, Lei L, Yoshimoto FK, Auchus RJ, Waterman MR, et al. Human cytochrome P450 21A2, the major steroid 21-hydroxylase: Structure of the enzyme•progesterone substrate complex and rate-limiting C-H bond cleavage. *J Biol Chem*. 2015;290(21):13128–43. doi:[10.1074/jbc.m115.646307](https://doi.org/10.1074/jbc.m115.646307)
38. Robinson PK. Enzymes: principles and biotechnological applications. *Essays Biochem*. 2015;59:1-41. doi:[10.1042/bse0590001](https://doi.org/10.1042/bse0590001)
39. Gay SC, Roberts AG, Halpert JR. Structural features of cytochromes P450 and ligands that affect drug metabolism as revealed by X-ray crystallography and NMR. *Future Med Chem*. 2010;2(9):1451-68. doi:[10.4155/fmc.10.229](https://doi.org/10.4155/fmc.10.229)
40. Hawkins CL, Davies MJ. Detection, identification, and quantification of oxidative protein modifications. *J Biol Chem*. 2019;294(51):19683-708. doi:[10.1074/jbc.rev119.006217](https://doi.org/10.1074/jbc.rev119.006217)
41. Poulos TL. Heme enzyme structure and function. *Chem Rev*. 2014;114(7):3919-62. doi:[10.1021/cr400415k](https://doi.org/10.1021/cr400415k)
42. Infield DT, Rasouli A, Galles GD, Chipot C, Tajkhorshid E, Ahern CA. Cation- $\pi$  Interactions and their Functional Roles in Membrane Proteins. *J Mol Biol*. 2021;433(17):167035. doi:[10.1016/j.jmb.2021.167035](https://doi.org/10.1016/j.jmb.2021.167035)